Supporting Information: Calcium inhibition of Ribonuclease H1 two-metal ion catalysis

Edina Rosta[1,2], Wei Yang[3], Gerhard Hummer[1,4]

[1]Laboratory of Chemical Physics, National Institute of Diabetes and Digestive and Kidney Diseases, National Institutes of Health, Bethesda, Maryland 20892-0520, U.S.A.

[2]Department of Chemistry, King's College London, London, SE1 1DB, United Kingdom

[3]Laboratory of Molecular Biology, National Institute of Diabetes and Digestive and Kidney Diseases, National Institutes of Health, Bethesda, Maryland 20892, U.S.A.

[4]Department of Theoretical Biophysics, Max Planck Institute of Biophysics, 60438 Frankfurt am Main, Germany

I. Methods

QM/MM Simulations.

The QM region included (see also Fig. S1) the RNA backbone from the ribose immediately upstream of the cleaved phosphodiester bond to the first and second phosphate group downstream (i.e., in the 3′ direction). In addition, the Mg^{2+} and Ca^{2+} ions were treated quantum mechanically, together with the carboxy-groups of Asp71, Glu109, Asp132, Glu188, and Asp192. We represented all Asp and Glu residues as acetates in the free energy simulations, whereas during the minimizations Asp residues were only represented as formates consistent with our earlier work [1]. The Ser133 sidechain was represented as a methanol molecule. With

Asp132 unprotonated, we can focus on the rate limiting first step in which the RNA backbone is cleaved, but the ribose leaving group is not yet protonated [2]. Finally, seven water molecules were included in the QM region of the simulations, resulting in a total of 100 atoms in the QM region. We used the standard protonation states of the ionizable residues.

Atomic Charge Calculations.

We used the Gaussian09 [3] program package coupled to CHARMM to calculate single point QM/MM energies for several divalent metal ions. We used the 6-31+G* basis set for H, C, O, P atoms. For the metal ions we used larger basis sets: 6-311++G** for Be, Mg, and Ca, aug-cc-pVTZ [4] for Mn, Ni, Fe, Co, Cr, and aug-cc-pVTZ-PP [5] for Cu, Zn, Pd, Cd, and Hg. We calculated all possible spin states for the d-orbitals with systems containing transition metal ions and found that the high spin states had the lowest energy in all cases in accordance with previous studies[6-8]. Singh-Kollman atomic charges [9] on the metal ions were determined with the ionic radii [10] corresponding to octahedral metal ion coordination in a high spin state (Table S3).

II. Active site and reaction coordinates

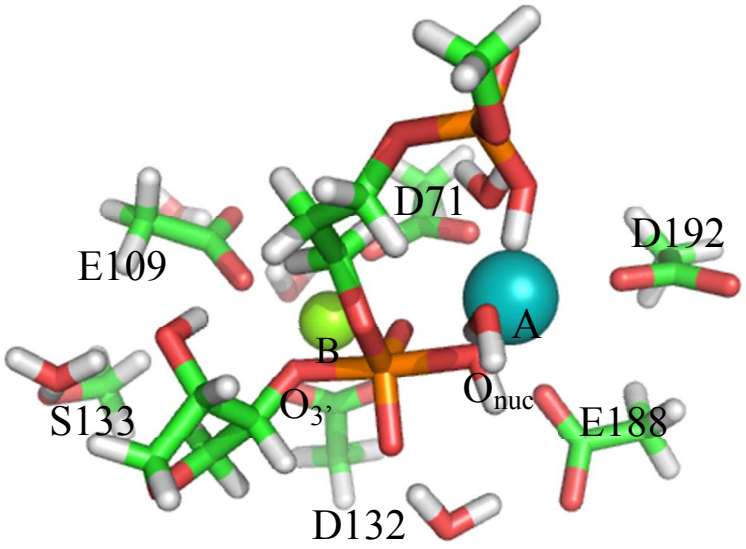

Figure S1. The QM region of the active site at a configuration near the transition state. Metal ion A coordinating the nucleophilic hydroxide is shown in light blue as a larger ion.

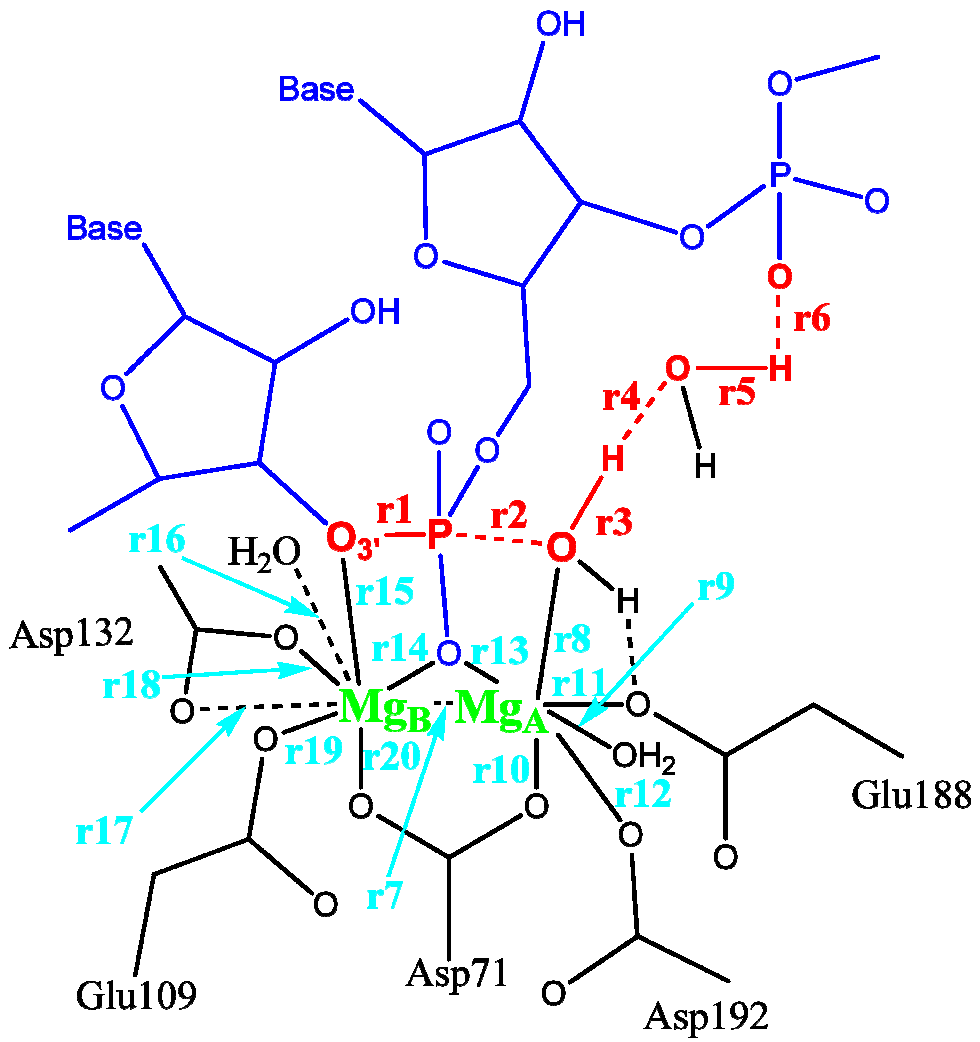

Figure S2. 20 coordinates used in the string free energy simulations. To analyze the results, we also defined a 2D projection via Q_e=r2-r1, and Q_p=0.5*(r3-r4+r5-r6), and a 1D projection as $Q_{ep}=Q_e+Q_p$.

Table S1. List of atom pairs in the 20 coordinates used in the string simulations. The atoms are defined according to the residue number given in the PDB structure 1ZBI.

	Atom 1	**Atom 2**
r1	A9 O3'	U10 P
r2	U10 P	Wat 303 O
r3	Wat 303 O	Wat 303 H
r4	Wat 303 H	Wat 52 O
r5	Wat 52 O	Wat 52 H
r6	Wat 52 H	U11 O1P
r7	Mg 301	Mg 302
r8	Mg 301	Wat 303 O
r9	Mg 301	Wat 304 O
r10	Mg 301	Asp71 OD2
r11	Mg 301	Glu188 OE2
r12	Mg 301	Asp192 OD2
r13	Mg 301	U10 O2P
r14	Mg 302	U10 O2P
r15	Mg 302	A9 O3'
r16	Mg 302	Wat 339 O
r17	Mg 302	Asp132 OD2
r18	Mg 302	Asp132 OD1
r19	Mg 302	Glu109 OE2
r20	Mg 302	Asp71 OD1

III. Free energy of Ca substituted systems

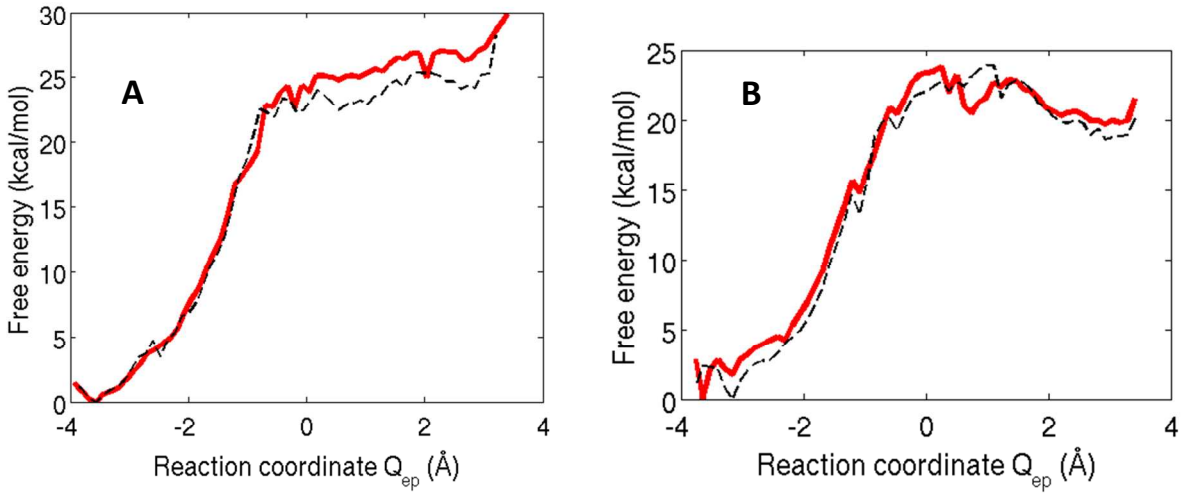

Figure S3. Free energy profiles of the CaMg (**A**) and MgCa (**B**) system. The 1D profile of the free energy corresponds to the projection onto Q_{ep} (red solid line). (For a definition of the reaction coordinates see Fig. S2.) **A.** We obtained a free energy barrier of about 25 kcal/mol using 125.52 ps total data, excluding the first 10 steps after each string update from the analysis. To test for convergence of the free energy barrier, free energy surfaces were recalculated with half the data (52.36 ps, black dashed line). **B.** We obtained a free energy barrier of about 24 kcal/mol using 125.74 ps total data, excluding the first 10 steps after each string update from the analysis. To test for convergence of the free energy barrier, free energy surfaces were recalculated with half the data (63.82 ps, black dashed line).

IV. Energy minimizations

We used the DFT B3LYP method with the 6-31+G* basis set to obtain the QM/MM minimized pathway. During the minimizations we used a 0.1 kcal/mol energy tolerance followed by 50 steps of additional minimizations and an additional minimization using 0.01 kcal/mol energy convergence tolerance. We found that the energetics and reaction pathways obtained from energy minimizations starting from equilibrated structures of the string simulations are overall consistent with the free energy calculations. The MgMg minimum energy barrier at Q_{ep}~0.5 Å is about ~19 kcal mol^{-1} compared to ~17 kcal mol^{-1} in the free energy [2]; for CaMg, it is ~24 kcal mol^{-1} vs ~25 kcal/mol in the free energy; and for MgCa we obtained ~25 kcal mol^{-1} vs. ~24 kcal mol^{-1} from free energy calculations.

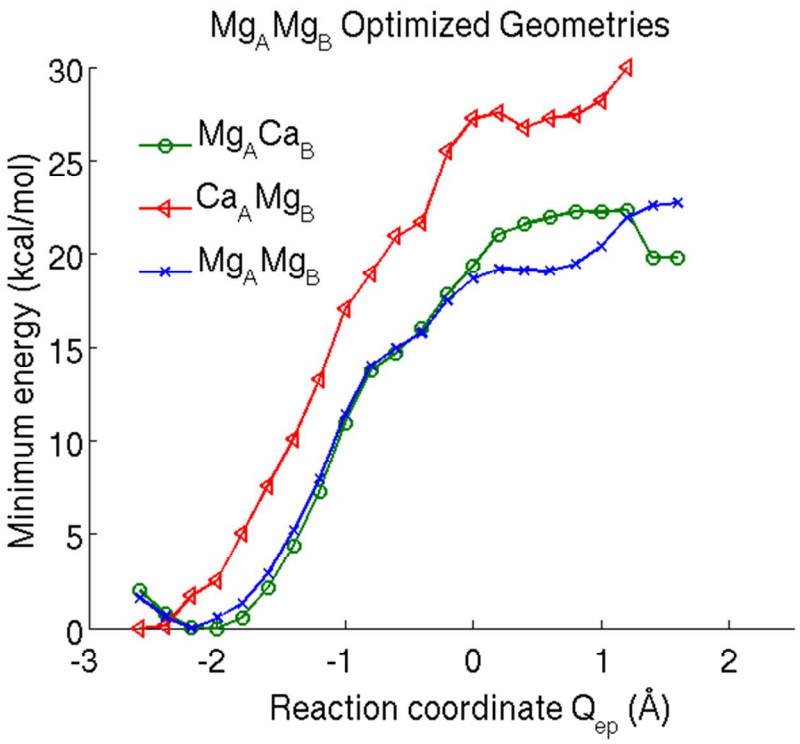

Figure S4. Energy minimized pathway for the MgMg system (blue, crosses). Single point QM/MM energies at the same level of theory are also shown for CaMg (red, triangles) and MgCa (green, circles) substituted systems using the coordinates obtained from the MgMg energy minimized pathway.

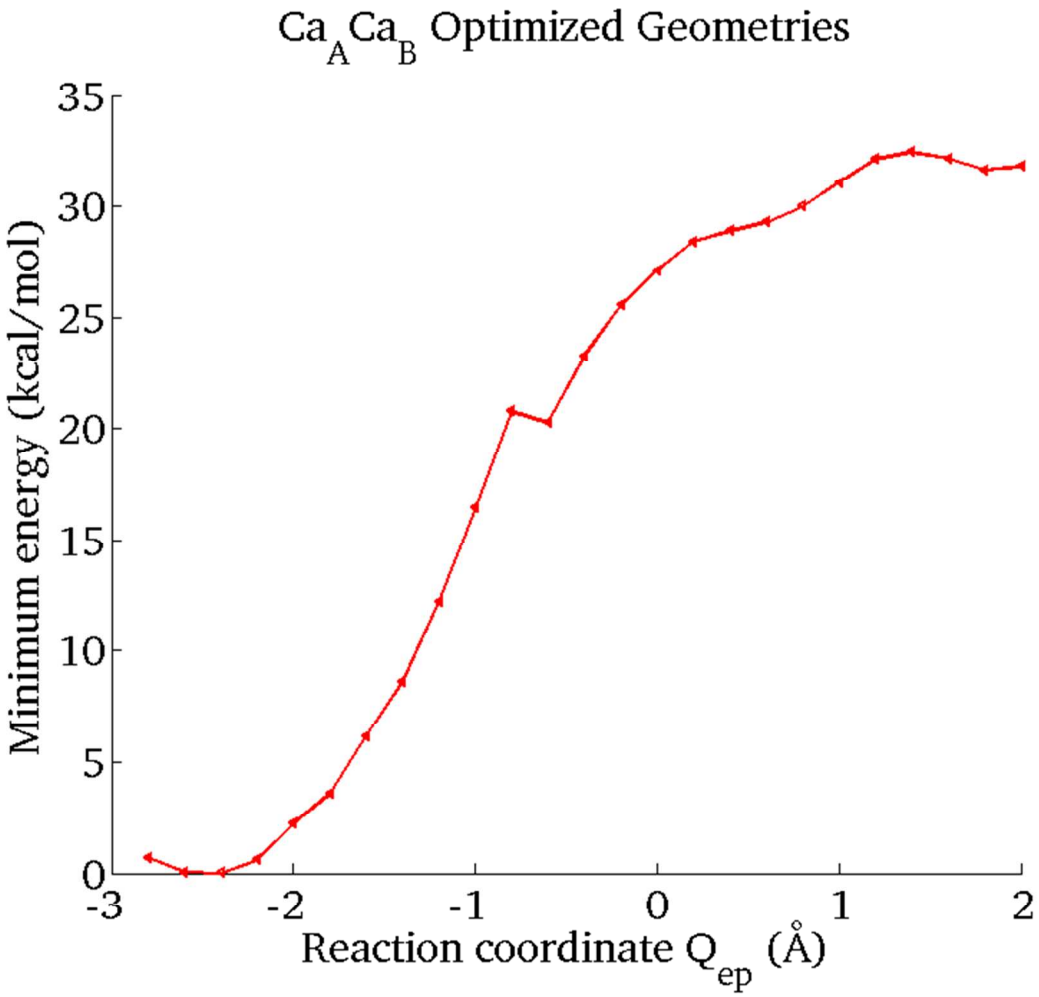

Figure S5. Energy minimized pathway for the CaCa system, with Ca^{2+} ions occupying the two metal ion binding sites.

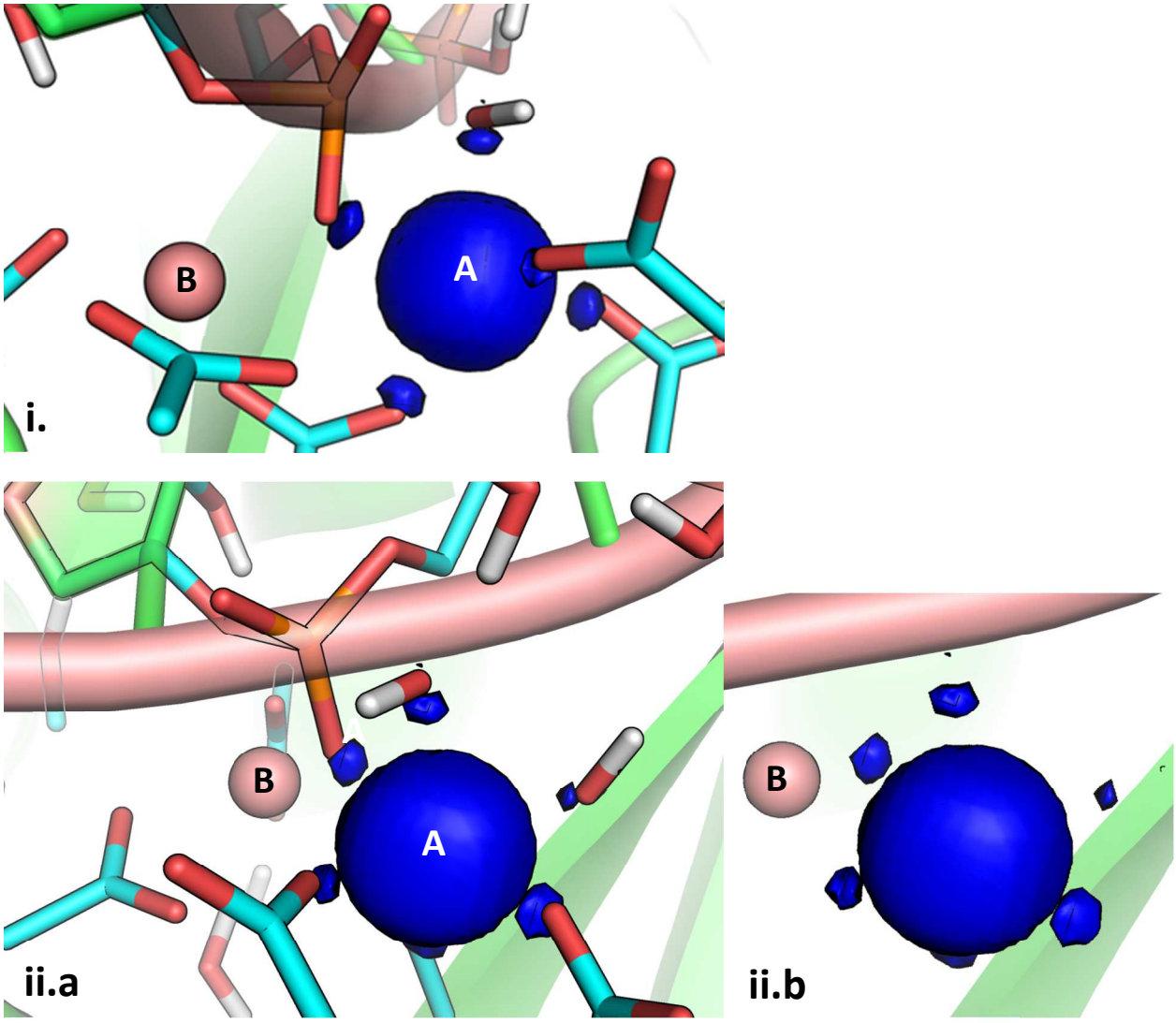

Figure S6. The total electron density difference between the CaMg and MgMg systems is drawn at the 0.01 contour level (blue; a.u.). Two different viewing angles are shown (i and ii), the stick representation is omitted in ii.b.

V. Metal ion coordination geometry

Table S2. Changes in metal-ligand and metal-metal distances upon substitution of Mg^{2+} by Ca^{2+}. Distances are listed for transition state structures were used from minimizations. Also listed are average distances for structures near the transition state in the string simulations.

Reaction Coordinate	Bonded atoms		Minimizations			String simulations	
			MgMg	MgCa	CaMg	MgCa	CaMg
7	Metal A	Metal B	**3.8**	**4.0**	**3.9**	**3.9**	**4.0**
8	Metal A	Wat 1 O	2.2	2.2	**2.4**	2.3	**2.5**
9	Metal A	Wat 2 O	2.2	2.3	**2.5**	2.3	**2.4**
10	Metal A	Asp71 OD2	2.1	2.1	**2.3**	2.0	**2.3**
11	Metal A	Glu188 OE2	2.1	2.1	**2.3**	2.2	**2.4**
12	Metal A	Asp192 OD2	2.1	2.1	**2.3**	2.1	**2.3**
13	Metal A	U10 O2P	2.1	2.1	**2.4**	2.1	**2.4**
14	Metal B	U10 O2P	2.1	**2.3**	2.1	**2.3**	2.0
15	Metal B	A9 O3'	2.4	**2.6**	2.6	**2.6**	2.3
18	Metal B	Asp132 OD1	2.1	**2.3**	2.1	**2.4**	2.1
19	Metal B	Glu109 OE2	2.1	**2.4**	2.0	**2.3**	2.1
20	Metal B	Asp71 OD1	2.0	**2.3**	2.0	**2.4**	2.1

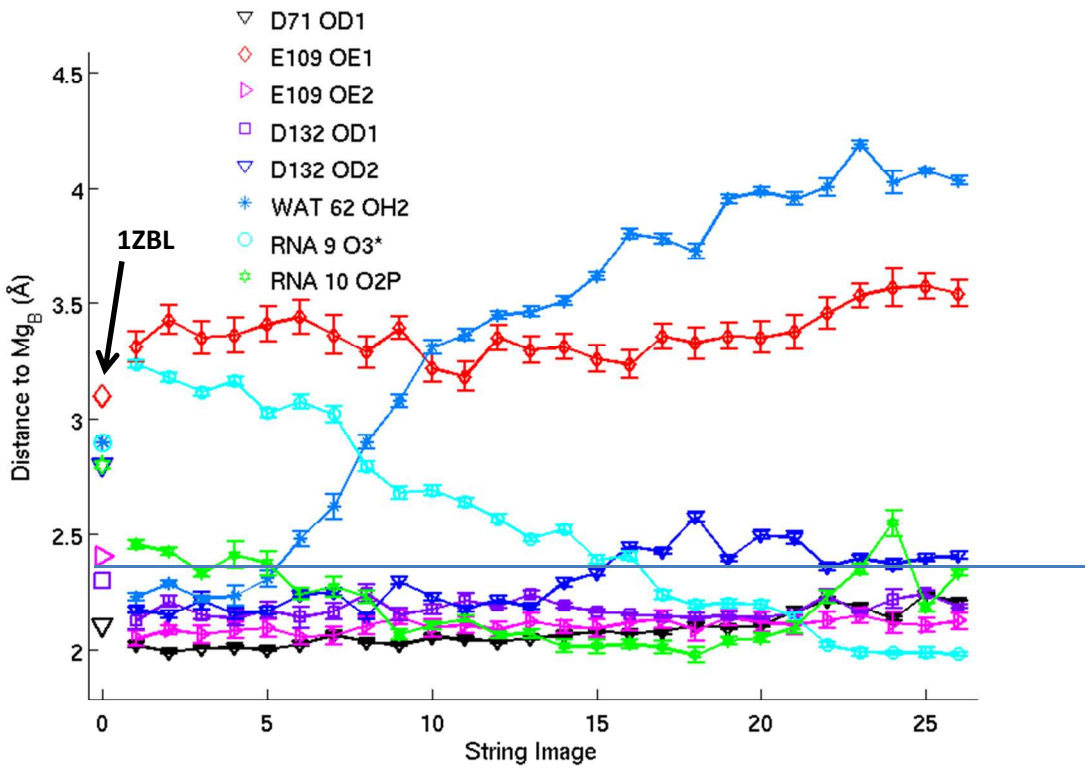

Figure S8. Metal ion B coordination in the CaMg string simulations along the reaction profile. Average distances between Mg_B and coordinating oxygen atoms are shown with error bars indicating their standard deviations, as calculated from the last 1.1 ps of simulation data in each string image. At the left, coordination distances are also given for the PDB structure 1ZBL for comparison.

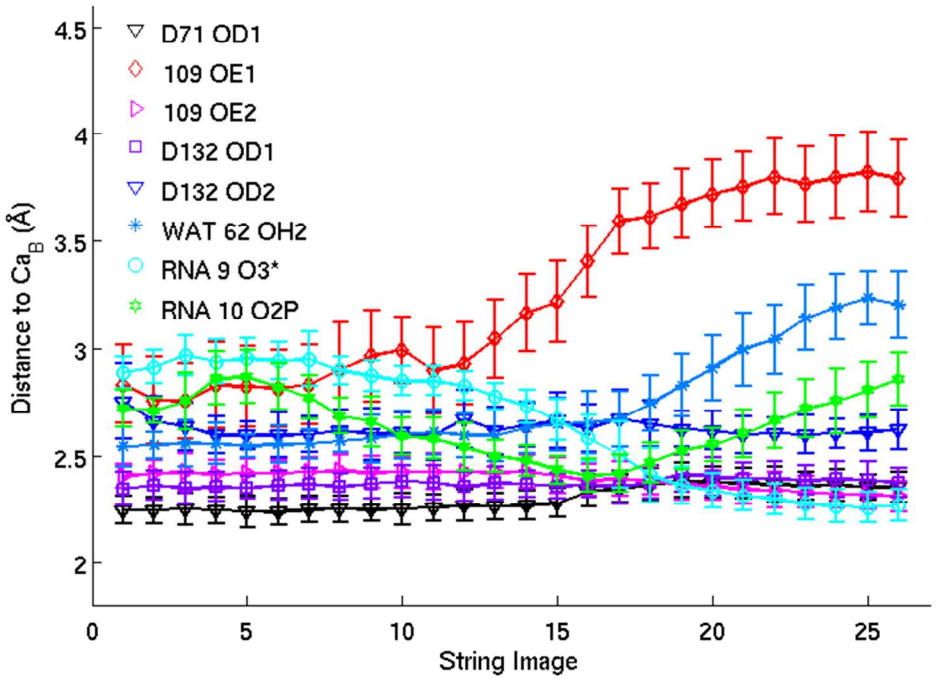

Figure S9. Metal ion B coordination in the MgCa string simulations. Average distances between Ca_B and coordinating oxygen atoms are shown with error bars indicating their standard deviations, as calculated from the last 1.1 ps of simulation data in each string image.

VI. Charge transfer and gas phase acidity

Table S3. Ionic radii, calculated reaction barriers for MgMg optimized reaction path, and atomic charges obtained for various metal ion replacements at binding site A in the reactant state (RS) and the transition state (TS).

Metal Ion	Ionic Radius[a]	Barrier[b]	α[c]	Atomic Charge[d] (e)	
				RS	TS
Mg^{2+}	72	19.0	0.172	1.9	1.8
Ca^{2+}	100	27.0	3.203	2.0	1.9

[a] in pm, ref. [10] [b] in kcal mol^{-1} [c] The metal ion polarizabilities (a.u.) and [d] Singh-Kollman atomic charges were calculated with Gaussian09.

Table S4. Energy barriers and metal ion charge for the initial RNase H cleavage reaction steps using Mg-optimized pathway. The QM/MM barrier is calculated as the total QM/MM energy difference, and the QM barrier is calculated as the difference between the polarized QM energies. The last two columns list the energy differences $\Delta E = E(Me^{2+}.OH^-) - E(Me^{2+}.H_2O)$ in units of kcal/mol to assess the gas-phase acidities of the metal ions. The energies were calculated for metal-ligand complexes with frozen geometries taken from optimized Mg-ligand complexes (nonopt), and for complexes whose structures were geometry optimized (opt).

Ion	QM/MM barrier[a]	QM barrier[a]	TS charge[a]	QM/MM barrier[b]	QM barrier[b]	RS charge[b]	TS charge[b]	Ion Size	ΔE (nonopt)	ΔE (opt)
Mg^{2+}	17.9	20.2	1.83	19.0	21.8	1.91	1.76	72	-95.0	-95.0
Ca^{2+}	26.7	29.0	1.92	27.0	30.8	2.02	1.89	100	-110.2	-109.1

[a]TS and RS chosen from MgMg system along the path

[b]TS and RS chosen along substituted metal ion path

VII. References

Complete author list for **reference 70**:

Shao, Y.; Molnar, L. F.; Jung, Y.; Kussmann, J.; Ochsenfeld, C.; Brown, S. T.; Gilbert, A. T. B.; Slipchenko, L. V.; Levchenko, S. V.; O'Neill, D. P.; Jr, R. A. D.; Lochan, R. C.; Wang, T.; Beran, G. J. O.; Besley, N. A.; Herbert, J. M.; Lin, C. Y.; Voorhis, T. V.; Chien, S. H.; Sodt, A.; Steele, R. P.; Rassolov, V. A.; Maslen, P. E.; Korambath, P. P.; Adamson, R. D.; Austin, B.; Baker, J.; Byrd, E. F. C.; Dachsel, H.; Doerksen, R. J.; Dreuw, A.; Dunietz, B. D.; Dutoi, A. D.; Furlani, T. R.; Gwaltney, S. R.; Heyden, A.; Hirata, S.; Hsu, C.-P.; Kedziora, G.; Khalliulin, R. Z.; Klunzinger, P.; Lee, A. M.; Lee, M. S.; Liang, W.; Lotan, I.; Nair, N.; Peters, B.; Proynov, E. I.; Pieniazek, P. A.; Rhee, Y. M.; Ritchie, J.; Rosta, E.; Sherrill, C. D.; Simmonett, A. C.; Subotnik, J. E.; Woodcock, H. L.; Zhang, W.; Bell, A. T.; Chakraborty, A. K.

Complete author list for **reference 73**:

Brooks, B. R.; Brooks, C. L.; Mackerell, A. D.; Nilsson, L.; Petrella, R. J.; Roux, B.; Won, Y.; Archontis, G.; Bartels, C.; Boresch, S.; Caflisch, A.; Caves, L.; Cui, Q.; Dinner, A. R.; Feig, M.; Fischer, S.; Gao, J.; Hodoscek, M.; Im, W.; Kuczera, K.; Lazaridis, T.; Ma, J.; Ovchinnikov, V.; Paci, E.; Pastor, R. W.; Post, C. B.; Pu, J. Z.; Schaefer, M.; Tidor, B.; Venable, R. M.; Woodcock, H. L.; Wu, X.; Yang, W.; York, D. M.; Karplus, M.

(1) Rosta, E.; Woodcock, H. L.; Brooks, B. R.; Hummer, G. *J. Comput. Chem.* 2009, *30*, 1634.

(2) Rosta, E.; Nowotny, M.; Yang, W.; Hummer, G. *Journal of the American Chemical Society* 2011, *133*, 8934.

(3) Frisch, M. J.*et. al* In *Gaussian 09, Revision B.01, Gaussian, Inc., Wallingford CT* Wallingford CT, 2009.

(4) Balabanov, N. B.; Peterson, K. A. *Journal of Chemical Physics* 2005, *123*, 064107.

(5) Peterson, K. A.; Puzzarini, C. *Theor. Chem. Acc.* 2005, *114*, 283.

(6) Cisneros, G. A.; Perera, L.; Garcia-Diaz, M.; Bebenek, K.; Kunkel, T. A.; Pedersen, L. G. *DNA Repair* 2008, *7*, 1824.

(7) Siegbahn, P. E. M. *Theor. Chem. Acc.* 2001, *105*, 197.

(8) Ivanov, I.; Klein, M. L. *Journal of the American Chemical Society* 2005, *127*, 4010.

(9) Singh, U. C.; Kollman, P. A. *J. Comput. Chem.* 1984, *5*, 129.

(10) Shannon, R. *Acta Crystallographica Section A* 1976, *32*, 751.